PAPER

Check for updates

Efficient adsorptive removal of potassium from potassium perrhenate solution using a cationic ion exchange resin†

Kunkun Chen, [ID] [ab] Linbo Li,*[a] Kai Yang,[a] Qigao Cao[b] and Yunfei Chen [ID] [b]

Potassium is a harmful impurity in the rhenium sinter, which adversely affects its mechanical properties by significantly reducing the density of sintered rhenium. Cationic resin is a promising material for potassium removal. In this study, the strong acid cationic exchange resin C160H was pretreated with an HNO_3 solution to enhance its performance in potassium removal. The pretreated C160H resin was characterized using BET, SEM and point of zero charge (PZC) measurements to understand its physicochemical properties. It was verified that the lower PZC value of C160H than that of pristine C160 resin resulted in increased potassium adsorption efficiency. Moreover, the pretreated C160H resin exhibited a maximum potassium adsorption efficiency of 99.28% for 2.00 g L^{-1} KReO$_4$ at 25 °C and pH 7.0 for 6 h, with a solid-to-liquid ratio of 1 : 20. The cation sequence affecting potassium adsorption efficiency was found to be Na$^+$ < Ca^{2+} < Fe^{3+} < NH$_4^+$. Isothermal adsorption thermodynamics showed that potassium adsorption by C160H resin followed a heterogeneous and exothermic process. The pseudo-second-order kinetics model best fitted the data, suggesting that potassium adsorption was primarily chemical in nature. DFT calculations confirmed that the adsorption mechanism was based on ion exchange between H$^+$ and K$^+$, with electrostatic interactions serving as the primary driving force for adsorption. The C160H resin demonstrated outstanding regeneration performance, maintaining an adsorption efficiency above 99% after ten cycles. These findings could contribute to improve the potassium adsorption capacity of the resin, thereby reducing both resin dosage and cost in the purification of perrhenate salts.

1. Introduction

Rhenium is a strategic refractory metal with a high melting point, high strength, corrosion resistance and other excellent properties, making it widely useable in aerospace, petrochemical and electronics industries.[1] Rhenium is primarily associated with molybdenite and chalcocite in nature. However, as primary rhenium resources become increasingly scarce, the recovery of rhenium from tungsten-rhenium alloy waste and other secondary resources has been extensively studied by researchers worldwide.[2–4] For recovery from tungsten–rhenium alloy waste, the main approach involves transferring rhenium from the waste to a solution, followed by the recovery of rhenium from the rhenium-containing solution.[4–6] Usually, potassium perrhenate is precipitated from the rhenium-containing solution using potassium salts to maximize the rhenium recovery ratio.

As is well known, the precursor for rhenium production is pure ammonium perrhenate salt. It is necessary to convert potassium perrhenate to ammonium perrhenate. Moreover, the presence of potassium impurity in ammonium perrhenate adversely affects the mechanical properties of rhenium sinter, as potassium significantly reduces the density of sintered rhenium.[7] Generally, sintered rhenium can be readily rolled into sheets or drawn into wires when the density exceeds 90% of the theoretical density. The density of sintered rhenium remains above 90% of the theoretical density when the potassium impurity level is below 0.006%. However, at a potassium impurity level of 0.41%, the density of the sintered rhenium decreases to 60% of the theoretical density, preventing the fabrication of sintered rhenium.[8,9]

Potassium impurities can be removed from ammonium perrhenate using several reported methods, such as precipitation, recrystallization, adsorption, liquid extraction and electrodialysis.[10,11] Zagorodnyaya *et al.*[12,13] compared the purification of crude ammonium perrhenate from potassium by recrystallization, sorption and membrane electrodialysis and indicated that it is impossible to produce 0.001 wt% potassium content of ammonium perrhenate using multi-stage recrystallization. Furthermore, the drawbacks of the recrystallization method are that it is energy-intensive and operation-intensive. Due to the low

[a]*School of Metallurgical Engineering, Xi'an University of Architecture and Technology, Xi'an 710055, China. E-mail: yj-lilinbo@xauat.edu.cn*

[b]*Electronic Material Research Center, Northwest Institute for Nonferrous Metal Research, Xi'an 710016, China*

† Electronic supplementary information (ESI) available. See DOI: https://doi.org/10.1039/d4ra08404g

solubility of potassium perrhenate in water, it is challenging to remove potassium by recrystallization from ammonium perrhenate. Palant[14] and Agapova[15] have investigated the electrodialysis of potassium perrhenate solutions to produce concentrated rhenium acid. The electrodialysis method requires a special construction electrodialyser and heterogeneous ionic membranes, limiting the industrial application of this method. The sorption method is the most promising method for purifying crude ammonium perrhenate, with the advantage of simple operation, high quality and yield of pure ammonium perrhenate. Leszczyńska-Sejda et al.[16] studied the sorption of ammonium ion from ammonium perrhenate solution using C160 cation resin to obtain perrhenic acid, and the potassium concentration was less than 0.2 mg L^{-1} in the obtained perrhenic acid, but the adsorption behavior of potassium was not reported. Zagorodnyaya et al.[11,12] investigated the purification of crude ammonium perrhenate solutions from potassium using KU-2 and KU-8 cation resins, and the concentration of potassium decreased from 38.6 mg L^{-1} to 0.192 mg L^{-1}, indicating that the removal efficiency of potassium was greater than 99%; finally, the obtained pure salt contained less than 0.001 wt% of potassium. Parizi et al.[17] employed C100 resin to study the isotherm and kinetic of potassium adsorption from ammonium perrhenate solutions. Although the potassium adsorption from ammonium perrhenate solution has been investigated by the above-mentioned researchers, few studies have focused on the adsorption properties and mechanisms of cationic ion exchange resins towards potassium from potassium perrhenate solutions.

Among the purification methods for the rhenium contained in aqueous solutions, ion exchange was the first technique widely used in the industry.[18] Various types of resins have been adopted in the separation and purification of rhenium, which can be reused after reactivation. A weak base anionic exchange resin, Purolite A170, and a strong base anionic exchange resin, D296, were used to separate rhenium from the copper leach solution and Mo–Re bearing solution, respectively.[19–21] However, anionic exchange resins were mainly employed to adsorb ReO$_4^-$ ions from the rhenium-containing solution and were unsuitable for removing potassium impurities. Generally, the removal of potassium was achieved by strong acid cation resins. Lucas et al.[22] reported that the potassium could be effectively uptaken by strong acid cationic exchange resins Dowex XZS-1 and Amberlite 252 from crude polyols. Zhang et al.[23] employed the cationic resin ZGC108 to effectively remove potassium ions from molasses vinasses, and the resin was pretreated with 1 mol L^{-1} HCl solution to convert the Na$^+$ form to the H$^+$ form. In addition to cationic resins, other sorbents were also used to remove potassium from industrial wastewater. Gołub et al.[24] investigated the removal of potassium impurity from wastewater with three sorbents, such as halloysite Halosorb, calcined diatomaceous earth Compakt and Damsorb K, and found that the removal efficiency of potassium reached 63.43–84.71% on Halosorb, 60.52–88.55% on Compakt, and 57.00–84.53% on Damsorb K. Owing to the low-cost, simple to use and superior potassium removal properties of the cationic ion exchange resin, the cation resin was selected to remove potassium from potassium perrhenate solutions in this study.

In the previous work,[25] the potassium removal efficiency of different types of cationic resins was determined from potassium perrhenate solutions to conclude the C160 resin (H$^+$ form) as the optimal adsorbent for removing potassium. The effects of solution acidity and feed flow rate on potassium removal efficiency were investigated by a column test. The breakthrough curve of the C160 resin (H$^+$ form) toward potassium was also investigated in the 10.0 g L^{-1} KReO$_4$ solution. The previous research mainly focused on optimizing the practical application process of removing potassium from potassium perrhenate solution by cationic resin. However, the adsorption behavior and mechanism of potassium removal from potassium perrhenate solution by C160 resin (H$^+$ form) are still unclear. In this work, the adsorption of potassium on C160H cationic resin in the batch (static) mode combined with theoretical calculations was systematically investigated to interpret the adsorption behavior and mechanism involved. Furthermore, the pretreated C160H resin was characterized by several analytical techniques and tested with different experimental parameters to determine the optimum potassium adsorption conditions from potassium perrhenate solution. The adsorption isotherms were established by using the influence of different initial potassium concentrations and temperature on the absorption capacity of potassium at equilibrium. The adsorption thermodynamics was studied to explain the nature of the potassium absorption process. The adsorption kinetics was also studied to determine the dominant adsorption steps. Finally, the regeneration experiments were employed to test the regeneration performance of the resin. The novelty of this study lies in understanding the intrinsic cause of the pretreated C160H resin with HNO$_3$ solution, improving the potassium removal efficiency and the adsorption behavior and mechanisms, which is important for increasing the potassium adsorption capacity of the resin to reduce the resin dosage and cost in the purification industry of perrhenate salts.

2. Materials and methods

2.1 Materials

In the previous work, the electrochemical dissolution method was used to dissolve tungsten–rhenium alloy waste in NaOH solution, and then the electrolytic solution was selectively separated using calcium chloride to precipitate tungsten and potassium chloride to precipitate rhenium.[26] Potassium perrhenate obtained from the solution after precipitation of tungsten was used to prepare the stock solution in this work, the composition of which is shown in Table 1.

The C160 resin purchased from Purolite (China) Co., Ltd (Zhejiang province, China) was used as the absorbent, and its physical and chemical properties are listed in Table S1.† Nitric acid (HNO$_3$, 65–68%), hydrochloric acid (HCl, 36–38%), ammonium hydroxide (NH$_3$, 25–28%), sodium chloride (NaCl, 99.5%), sodium hydroxide (NaOH, 96%), ammonium chloride

Table 1 Chemical composition of potassium perrhenate, wt%

K	Na	Ca	Fe	W	Mo	Re
13.06	0.48	<0.01	<0.01	<0.01	<0.01	62.98

(NH$_4$Cl, 99.5%), calcium chloride anhydrous (CaCl$_2$, 96%), and iron trichloride hexahydrate (FeCl$_3$·6H$_2$O, 99%) were provided by Sinopharm Chemical Reagent Co., Ltd (Shanghai, China). All reagents were of analytical grade without further treatment. Deionized water (18.25 MΩ) was utilized throughout the experiments for solution preparation and resin washing.

The stock solutions containing 0.05 g L^{-1}, 0.10 g L^{-1}, 0.50 g L^{-1}, 1.00 g L^{-1}, 2.00 g L^{-1} KReO$_4$ were prepared by dissolving 0.005 g, 0.01 g, 0.05 g, 0.10 g, 0.20 g of potassium perrhenate in 100 mL of deionized water, respectively. The KReO$_4$ solution containing competing cations (Na$^+$, NH$_4^+$, Ca^{2+}, Fe^{3+}) were prepared with NaCl, NH$_4$Cl, CaCl$_2$ and FeCl$_3$·6H$_2$O dissolved in 2.00 g L^{-1} KReO$_4$ solution, respectively.

In order to convert the fresh C160 resin to the H$^+$ form, a pre-treatment step was performed prior to the experiments to eliminate any possible residual impurity of the resin and to obtain H$^+$ exchangeable ions. A certain amount of the C160 resin was washed repeatedly with deionized water to remove impurities. Then, the resin was immersed in a three-fold resin volume of 3 mol L^{-1} HNO$_3$ solution for 24 h. Subsequently, the resulting H$^+$ form resin was washed to neutral with deionized water and filtered. The obtained wet resin was stored in a capped plastic container for experimental use. For convenience, the obtained H$^+$ form resin was denoted as C160H.

2.2 Adsorption and regeneration experiments

Static experiments were carried out to assess the potassium adsorption efficiency of resins before and after pre-treatment. 5.0 g of C160 or C160H wet resin and 100 mL 2.00 g L^{-1} KReO$_4$ solution were placed in a 250 mL conical flask for shaking for 6 h at 25 °C and 180 rpm rotating speed. Subsequently, the initial pH of the KReO$_4$ stock solution was measured as 6.93 (approximately 7.0), and 1 M HCl was used to adjust the initial pH to 1.0, 3.0 and 5.0, and 1 M NH$_3$ H$_2$O was used to adjust the initial pH to 9.0 and 11.0. Then, a pH dependence study was conducted by adding 5.0 g of C160H resin to 100 mL 2.00 g L^{-1} KReO$_4$ solution with a pH of 1.0–11.0 for shaking for 6 h at 25 °C and 180 rpm. The effects of the solid-to-liquid ratio (1 : 50, 1 : 40, 1 : 30, 1 : 20, 1 : 10), adsorption temperature (15 °C, 25 °C, 35 °C, 45 °C, 55 °C) and adsorption time (0.5 h, 1 h, 1.5 h, 3 h, 6 h, 12 h, 24 h, 36 h) were also studied. The effect of competing cation (Na$^+$, NH$_4^+$, Ca^{2+}, Fe^{3+}) concentrations on the potassium adsorption efficiency of the C160H resin was studied at the initial K$^+$ concentration of 270 mg L^{-1} with the competing cation concentrations of 135, 270, 540 mg L^{-1}, respectively. The potassium concentration in the adsorbed solution was measured using an inductively coupled plasma atomic emission spectrometer (ICP-AES, iCAP 7000, Thermo, USA), and the potassium adsorption efficiency of C160 or C160H resin was calculated as follows:

$$\eta = \frac{(C_0 - C_e)}{C_0} \times 100\% \tag{1}$$

where η is the potassium absorption efficiency, %; C_0 is the initial concentration of potassium, mg L^{-1}; C_e is the concentration of potassium at equilibrium, mg L^{-1}.

During the isothermal experiments, 5.0 g of the C160H wet resin was weighed and mixed with 100 mL of 0.05 g L^{-1}, 0.10 g L^{-1}, 0.50 g L^{-1}, 1.00 g L^{-1}, and 2.00 g L^{-1} KReO$_4$ stock solution in a 250 mL conical flask, respectively. Then, the conical flask was placed in a water bath shaker, with the temperature controlled at 15 °C, 25 °C, 35 °C, 45 °C, and 55 °C and the rotating speed at 180 rpm. After shaking for 24 h, the supernatant was taken to analyze the potassium concentration using ICP-AES. For the adsorption isotherm, the details of the isotherm model are shown in Text S1.†

During kinetics experiments, the concentration of the stock solution was fixed at 2.0 g L^{-1}; other experimental conditions were the same as above. At selected time intervals, 0.5 mL of the solution was quickly sampled and diluted in a 25 mL volumetric flask to analyze the potassium concentration using ICP-AES. The adsorption kinetic curves were fitted according to the models shown in Text S2.† The equilibrium adsorption capacity (q_e) and adsorption capacity at time t (q_t) of the C160H resin for potassium were calculated as follows:

$$q_i = \frac{(C_0 - C_i)V}{m} \tag{2}$$

where q_i is the absorption capacity at equilibrium or at time t (min), mg g^{-1}; V is the volume of the stock solution, L; m is the adsorbent mass, g; C_0 is the initial concentration of potassium, mg L^{-1}; C_i is the concentration of potassium at equilibrium or at time t (min), mg L^{-1}.

Regeneration experiments were carried out using the batch and column tests, respectively. During the batch test, 5.0 g of the C160H wet resin was added to a conical flask containing 100 mL of potassium perrhenate solution with an initial concentration of 0.5 g L^{-1}. The mixture was shaken for 6 h at 25 °C and 180 rpm of rotating speed, and then the solution was separated for analyzing potassium concentration using ICP-AES. Subsequently, the resin was desorbed with 50 mL of 3 mol L^{-1} HNO$_3$ solution for shaking for 6 h at 25 °C and 180 rpm of rotating speed. In the next adsorption–desorption cycle, the resin was reused under the same conditions.

During the column test, a glass column of D12 mm × L300 mm was filled with 5.0 g of the C160H wet resin, then 100 mL of potassium perrhenate solution was pumped into the column by the peristaltic pump with 20 mL h^{-1} of flow speed at 25 °C. The initial concentration of the feeding solution was 0.5 g L^{-1}. After the adsorption, the effluent was sampled to analyze the potassium concentration using ICP-AES. The loaded resin was rinsed to neutral with deionized water, followed by desorption with 50 mL of 3 mol L^{-1} HNO$_3$ solution at 10 mL h^{-1} of flow speed. Subsequently, the regenerated resin was used in the next cycle. The batch and column regeneration processes were repeated ten times, respectively.

2.3 Characterization methods

The pore parameters of the resin before and after pre-treatment were determined by a mercury intrusion porosimetry (MIP) instrument (AutoPore IV9620, Micromeritics, USA) and an automatic specific surface area and porosity analyzer (NOVA

Paper   **RSC Advances**

touch 2LX, Quantachrome, USA). The Brunauer–Emmett–Teller (BET) method was used to calculate the specific surface area, while the pore distribution was determined by the Barrett–Joyner–Halenda (BJH) method. The Fourier transform infrared spectroscopy (FT-IR) of the resin before and after adsorption was obtained from a spectrometer (Nicolet6700, Thermo, USA) with a scanning range of 4000–400 cm^{-1}. The surface morphology and element mapping of the resin were obtained using a scanning electron microscope-energy dispersive spectrometer (SEM-EDS, SU6600, Hitachi, Japan). An organic element analyzer (UNICUBE, Elementar, Germany) was employed to characterize the resin before and after potassium adsorption.

The point of zero charge (PZC) of the resin before and after pre-treatment was determined using a pH meter (PHS-3C, Rex, China) using the solid addition method.[27,28] In a series of 50 mL centrifuge tubes, a set of 0.01 M NaCl solutions was adjusted to pH 1, 3, 5, 7, 9, and 11 with 0.1 M HCl and 0.1 M NaOH. The initial pH (pH$_i$) was recorded, and 0.2 g of the resin was added to 40 mL of each solution. The tubes were placed on a shaker and the final pH (pH$_f$) was measured after shaking for 24 h at 25 °C. The PZC was obtained from the plot of ΔpH (=pH$_f$–pH$_i$) against pH$_i$.

2.4 Density functional theory (DFT)

DFT theoretical calculations were performed using the Gaussian 16 program package. In order to expedite the calculation process, 4-styrenesulfonic acid was used as a surrogate

for the C160H resin. Full geometry optimizations were performed to locate all the stationary points using the B3LYP method with the 6-31G(d) basis, namely B3LYP/6-31G(d). Dispersion corrections were computed with Grimme's D3(BJ) method in optimization. Harmonic vibrational frequency was calculated at the same level to guarantee no imaginary frequency in the molecules, *i.e.*, they are located on the minima of the potential energy surface. After the structural optimization and frequency calculation, natural bond orbital (NBO) was further conducted to obtain the charge distributions.

3. Results and discussion

3.1 Characterization of resins before and after pre-treatment

3.1.1 Pore structure analysis. The pore structures of the C160 resin (before pre-treatment) and C160H resin (after pre-treatment) were first investigated through mercury intrusion porosimetry (MIP) since the commercial C160 resin has a macroporous structure (Table S1†). As shown in Fig. 1(a) and (b), macroporous and mesoporous structures coexisted in the C160 resin and C160H resin. However, after pre-treatment in 3 mol L^{-1} HNO$_3$ solution, the macroporous distributions had no obvious changes for the C160H resin, but the range of mesoporous distributions increased with decreased pore volume, indicating that the pre-treatment with nitric acid can improve the mesoporous structure of the C160 resin but not for the macroporous structure.

To further investigate the mesoporous structural changes, the BET surface area and pore size of C160 resin and C160H
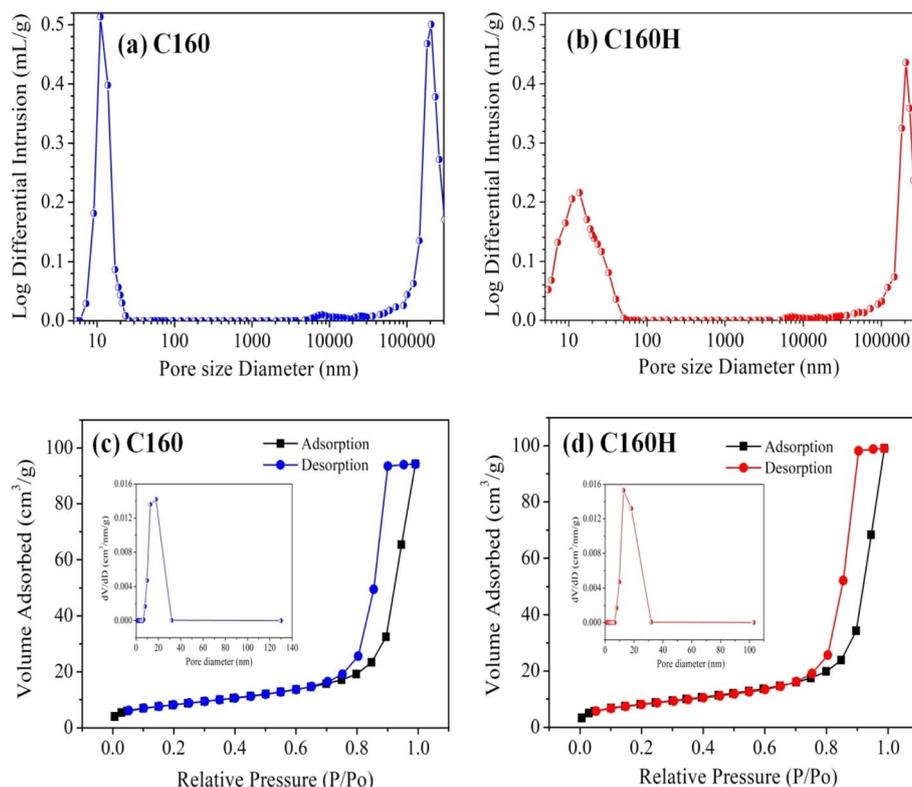

Fig. 1 Pore size distributions of C160 and C160H resins determined by mercury intrusion (a and b) and nitrogen adsorption (c and d).

Table 2 Pore parameters of the resins before and after pre-treatment

Resin	BET-specific surface area (m^2 g^{-1})	Total pore volume (cm^3 g^{-1})	Average pore size (nm)
C160	29.155	0.146	20.049
C160H	29.545	0.154	20.797

resin were tested through N$_2$ adsorption–desorption experiments, as shown in Fig. 1(c) and (d). According to the IUPAC standards, the N$_2$ adsorption–desorption isotherms exhibited an obvious H1-type hysteresis loop, indicating that both C160 resin and C160H resin have a mesoporous structure.[29] Moreover, Table 2 shows the porous parameters of the resins before and after pre-treatment, including the specific surface area, total pore volumes and average pore sizes. By comparing these parameters, it is found that the BET-specific surface area, total pore volumes and average pore sizes of the pretreated resin are slightly increased, which may be caused by the corrosion of the resin skeleton in nitric acid.[30]

3.1.2 SEM-EDS. The morphology changes of resins before and after pre-treatment were characterized by SEM (Fig. 2). Obviously, the resins exhibited a good spherical shape with a mean diameter of about 0.45 mm. The number and size of the surface pores of the C160H resin are greater than that of the C160 resin, which is consistent with the BET analysis results. The types and contents of elements in C160 and C160H resins were also examined using EDS patterns. C, O, S and Na elements

all existed in the C160 resin. However, the Na element could not be detected for the C160H resin, indicating that the C160 resin has been successfully converted into the H$^+$ form.

3.1.3 Point of zero charge (PZC). The point of zero charge is defined as the pH value at which the sorbent surface charge is equal to zero at some ambient temperature, applied pressure, and aqueous solution composition.[31] Sorbents with low PZC values would be best suited to capture cations, while sorbents with high PZC values would be more appropriate to capture anions.[28] Therefore, PZC values could help optimize the selection of resin for removing potassium.

The curves of ΔpH $vs.$ pH$_i$ for C160 and C160H resin obtained following the solid addition method are presented in Fig. 3. The PZC occurs at the point where ΔpH = 0. In 0.01 M NaCl, the PZC values of C160 and C160H resin were 6.19 and 1.63, respectively. The results show that the C160H resin owns a lower PZC value than the C160 resin. Therefore, the C160H resin is more appropriate to capture potassium cations from the view of PZC.

3.1.4 Potassium adsorption efficiency. To compare the potassium adsorption efficiency of resins before and after pre-treatment, the adsorption tests were conducted in batch experiments. As shown in Fig. S1,† the potassium adsorption efficiency on the C160 and C160H resin was 96.21% and 99.19%, respectively, suggesting that the potassium adsorption efficiency could be improved by pre-treating the C160 resin with nitric acid. This is mainly attributed to the lower PZC value of the C160H resin than the C160 resin, resulting in stronger
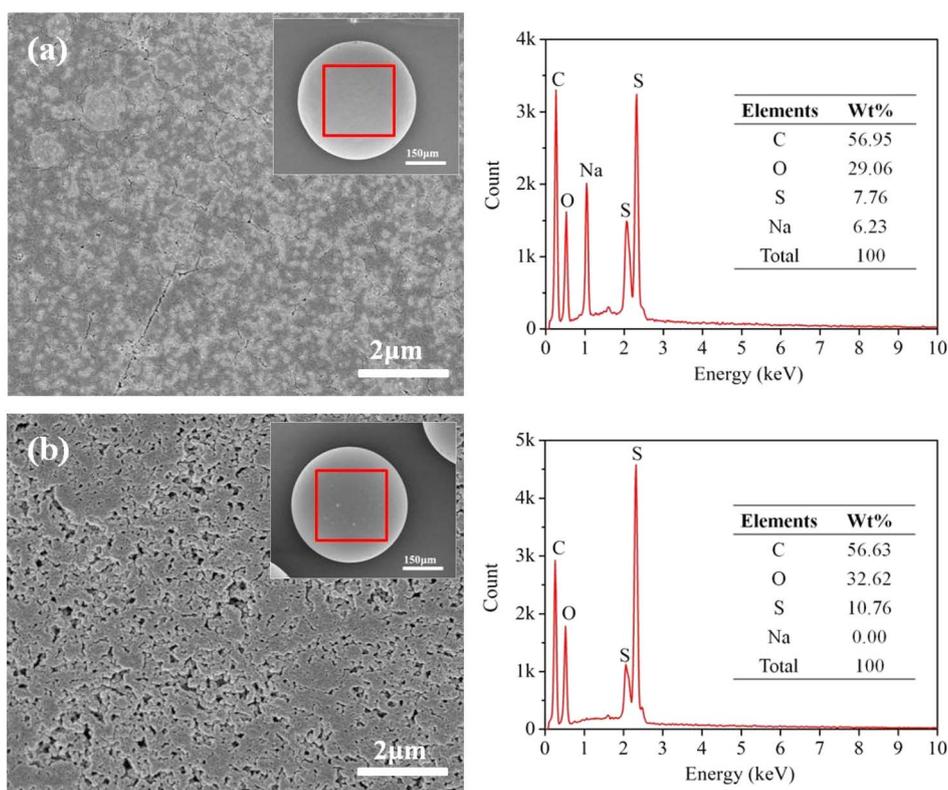

Fig. 2 SEM images and EDS pattern of C160 (a) and C160H resin (b).
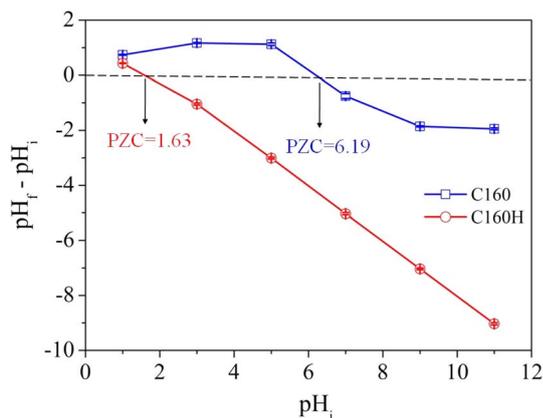
Fig. 3 Plots of ΔpH vs. pH_i for the solid addition method in 0.01 M NaCl.

deprotonation or ionization of functional groups and electrostatic interaction with potassium cations.[32,33] In addition, a slightly improved mesoporous structure may cause faster mass transfer of potassium cations in the C160H resin than in the C160 resin, increasing the potassium adsorption efficiency. It can also avoid the introduction of sodium impurity into the perrhenic acid after the ion exchange of potassium perrhenate solution using C160H resin.

3.2 Factors affecting adsorption

3.2.1 Effect of the solid-to-liquid ratio. The effect of the solid-to-liquid ratio, i.e., C60H resin dosage at fixed volumes of stock solution, on potassium adsorption efficiency is shown in Fig. 4(a). The adsorption efficiency increases rapidly as the solid-to-liquid ratio increases (i.e., the resin dosage increases). When the solid-to-liquid ratio is 1 : 20, the potassium adsorption efficiency is 99.28%. However, the potassium adsorption efficiency is lower than 99% as the solid-to-liquid ratio is below 1 : 20. This is not appropriate since potassium element is a harmful impurity in ammonium perrhenate, which adversely affects the mechanical properties of the subsequent rhenium sinter.[10] In addition, considering the resin cost, the solid-to-liquid ratio of 1 : 20 was used in all subsequent adsorption experiments.

3.2.2 Effect of initial pH and competitive cations. The effect of initial pH on the adsorption of potassium by C160H resins is illustrated in Fig. 3(b). The maximum potassium adsorption efficiency was obtained as 99.28% at pH = 7, and the potassium adsorption efficiency decreased gradually as the pH decreased to 1 or increased to 11. The potassium adsorption efficiency did not change visibly in the pH range of 3 to 9, indicating that C160H could be used as a potassium adsorbent in a wide pH range. In general, when the initial pH of a solution is less than the PZC value, the surface charge of the resin tends to be positive due to the protonation of the acidic groups, and potassium cation sorption is restricted due to electrostatic repulsion. Contrarily, when the initial pH of a solution is greater than the PZC value, the surface charge of the resin tends to be negative due to the deprotonation or ionization of the acidic

groups, and potassium cation sorption is enhanced due to electrostatic attraction.[33,34] The point of zero charge (PZC) of the C160H resin was obtained at pH 1.63. As pH > PZC, the negatively charged resin surface will facilitate the adsorption of potassium cations due to electrostatic attraction. The potassium adsorption efficiency increased with the initial pH increasing from 3 to 7, which resulted from the desorption of more protons from the resin surface to enhance the electrostatic attraction force. Moreover, Fig. 4(b) shows that the final pH is about 2.0, close to the PZC value in the initial pH range of 3 to 7, implying maximum electrostatic attraction as the resin surface released the most protons at a pH of 7. However, when pH dropped to 1, the potassium adsorption efficiency declined rapidly to 91.74%, resulting from the competition of H^+ or H_3O^+ ions with K^+ ions for active sites.[35] As the pH reached 9 and 11, the potassium adsorption efficiency decreased to 99.05% and 95.44%, respectively. This can be caused by the increased concentration of NH_4^+ due to adjusting the pH of the solution by adding ammonia. For these reasons, the potassium adsorption efficiency obtained the maximum value of 99.28% at pH = 7. Therefore, the following experiments were all conducted at an initial pH of 7.

An additional consideration for the practical application of the C160H resin is the selective adsorption of potassium in an environment where competitive cations, such as Na^+, NH_4^+, Ca^{2+} and Fe^{3+}, coexist. As shown in Table 1, the main impurities of potassium perrhenate include Na, Ca and Fe. Moreover, the concentration of K, Na, Ca and Fe in ammonium perrhenate was reported as 0.088–3.40%, 0.02–0.022%, 0.003–0.02%, and 0.001–0.3%, respectively.[12,17] Therefore, the potassium adsorption efficiency was analyzed using $KReO_4$ solutions of 270 mg L^{-1} K^+ with 135, 270, 540 mg L^{-1} Na^+, NH_4^+, Ca^{2+} or Fe^{3+} to evaluate the potassium selectivity of the C160H resin, as displayed in Fig. 4(c). C160H resin exhibited a high potassium adsorption efficiency of 99.20% when only K^+ was present, decreasing slightly to 97.66%, 97.72% and 97.53% when 270 mg L^{-1} Na^+, Ca^{2+} or Fe^{3+} was present. However, the potassium adsorption efficiency decreased to 96.82% when 270 mg L^{-1} NH_4^+ was present. The higher concentration of Na^+, NH_4^+, Ca^{2+} and Fe^{3+} leads to lower K^+ adsorption. The NH_4^+ has a most significant impact on potassium adsorption, and the lowest potassium adsorption efficiency in the tested condition was 93.24% for coexisting 540 mg L^{-1} NH_4^+. In addition, the cation competition sequence that affects the potassium adsorption efficiency was $Na^+ < Ca^{2+} < Fe^{3+} < NH_4^+$. The low potassium adsorption efficiency in the coexistence of NH_4^+ is attributed to the negligible size exclusion effect since the size of the hydrate NH_4^+ (3.31 Å) is equal to the K^+ size (3.31 Å), while the Na^+ (3.58 Å), Ca^{2+} (4.12 Å) and Fe^{3+} (4.57 Å) are comparably bigger than that of hydrate K^+.[36,37] The size exclusion effect would effectively happen for Na^+, Ca^{2+} and Fe^{3+}. Moreover, cationic exchange resins generally exhibit high selectivity toward multivalent cations and low selectivity for monovalent cations such as Na^+.[38] Therefore, the ion-exchange force on C160H decreased gradually for Fe^{3+}, Ca^{2+} and Na^+.

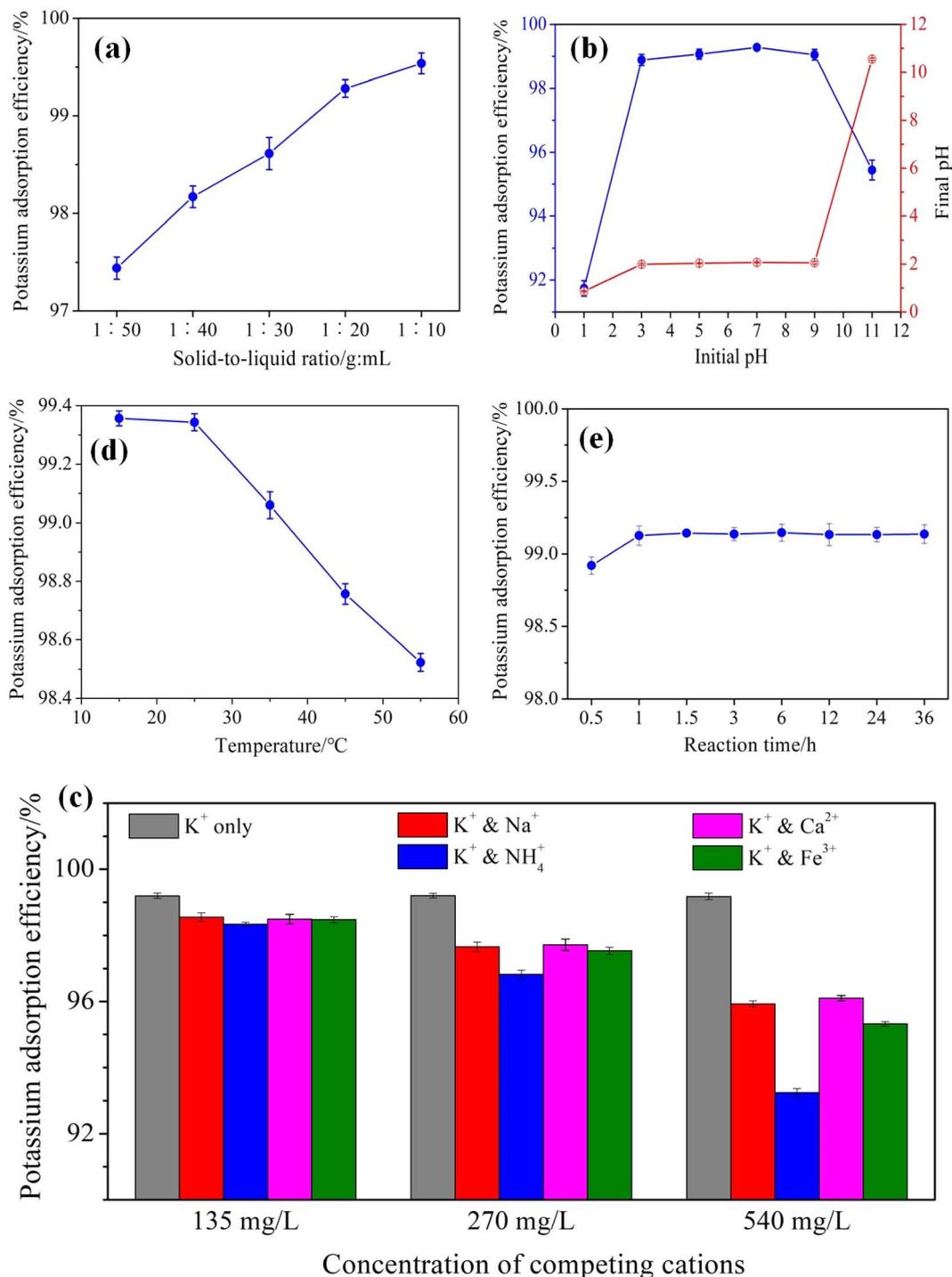**3.2.3 Effect of reaction temperature and time.** The effects of different adsorption temperatures on potassium adsorption

Fig. 4 Effect of various factors on potassium adsorption by the C160H resin from 2.00 g L^{-1} of KReO$_4$ solution (conditions for (a): initial pH = 7.0, temperature = 25 °C, rotating speed = 180 rpm, time = 6 h; conditions for (b): S/L = 1 : 20 g mL^{-1}, temperature = 25 °C, rotating speed = 180 rpm, time = 6 h; conditions for (c): initial pH = 7.0, S/L = 1 : 20 g mL^{-1}, temperature = 25 °C, rotating speed = 180 rpm, time = 6 h; conditions for (d): initial pH = 7.0, S/L = 1 : 20 g mL^{-1}, rotating speed = 180 rpm, time = 6 h; conditions for (e): initial pH = 7.0, S/L = 1 : 20 g mL^{-1}, temperature = 25 °C, rotating speed = 180 rpm).

efficiency are shown in Fig. 4(d). It can be concluded that the temperature has an adverse effect on the adsorption process. The thickness of the boundary layer surrounding the resin decreases as the temperature rises, resulting in a decrease in the surface activity of the resin and an increase in the tendency of

adsorbed potassium to release from the surface of the resin.[17] However, the effect of temperature on potassium adsorption efficiency was not obvious at the temperature below 25 °C. Moreover, the potassium perrhenate solid may be crystallized from the adsorption solution at a cooler temperature due to the

Table 3 Isotherm constants for different models of potassium adsorption on C160H resin

Model	Parameter		288 K	298 K	308 K	318 K	328 K
			T/K				
Langmuir	Fitting equation		$q_e = \dfrac{10.6474C_e}{1+1.2631C_e}$	$q_e = \dfrac{10.6628C_e}{1+1.3797C_e}$	$q_e = \dfrac{6.8439C_e}{1+0.8525C_e}$	$q_e = \dfrac{5.5166C_e}{1+0.6574C_e}$	$q_e = \dfrac{4.9679C_e}{1+0.6284C_e}$
	$q_{max}/(mg\ g^{-1})$		8.430	7.728	8.028	8.392	7.905
	$K_L/(L\ mg^{-1})$		1.263	1.380	0.852	0.657	0.628
	R^2		0.9872	0.9989	0.9850	0.9839	0.9838
Freundlich	Fitting equation		$q_e = 4.3635C_e^{1/1.776}$	$q_e = 4.1092C_e^{1/1.811}$	$q_e = 3.3746C_e^{1/1.833}$	$q_e = 3.040C_e^{1/1.835}$	$q_e = 2.7984C_e^{1/1.915}$
	$K_F/((mg\ g^{-1})\cdot(mg\ L^{-1})^{1/n})$		4.364	4.109	3.375	3.040	2.798
	n		1.776	1.811	1.833	1.835	1.915
	R^2		0.9962	0.9913	0.9982	0.9977	0.9986
Temkin	Fitting equation		$q_e = 4.3117 + 0.9647\ln C_e$	$q_e = 4.0762 + 0.9466\ln C_e$	$q_e = 3.7479 + 0.8375\ln C_e$	$q_e = 3.6914 + 0.8984\ln C_e$	$q_e = 3.5056 + 0.8268\ln C_e$
	$K_T/(L\ mg^{-1})$		87.304	74.138	87.811	60.869	69.395
	$B_T/(J\ mol^{-1})$		0.965	0.947	0.837	0.898	0.827
	R^2		0.8544	0.8609	0.8364	0.8375	0.8288
Dubinin–Radushkevich	Fitting equation		$\ln q_e = 1.3968 - 0.0259\varepsilon^2$	$\ln q_e = 1.3510 - 0.026\varepsilon^2$	$\ln q_e = 1.2504 - 0.0213\varepsilon^2$	$\ln q_e = 1.2716 - 0.0233\varepsilon^2$	$\ln q_e = 1.2111 - 0.0201\varepsilon^2$
	$q_m/(mg\ g^{-1})$		4.042	3.861	3.492	3.566	3.357
	$K_{DR}/(mol^2\ kJ^{-2})$		0.026	0.026	0.021	0.023	0.020
	R^2		0.9281	0.9580	0.9249	0.9283	0.9276

poor solubility of potassium perrhenate at low temperatures.[39] Therefore, the regeneration experiments were all conducted at 25 °C.

Fig. 4(e) shows the effects of adsorption time on potassium adsorption efficiency. The potassium adsorption efficiency did not change with the extension of adsorption time after 1 h, indicating that the equilibrium of potassium adsorption on the C160H resin was established after 1 h. This was essential to obtain rapid kinetics for potassium adsorption when designing adsorption systems, ensuring a better adsorption process economy. Nevertheless, in order to ensure that the equilibrium is reached, a 24 h shaking time was selected for adsorption isotherm experiments.

3.3 Potassium adsorption behavior

3.3.1 Adsorption isotherms. The isothermal adsorption was conducted with various initial concentrations of potassium perrhenate solution. The equilibrium data of potassium adsorption on the C160H resin were analyzed separately by fitting data to Langmuir, Freundlich, Temkin, and Dubinin–Radushkevich isotherm equations, as shown in Fig. S2.† The values of parameters related to the Langmuir and Freundlich models are obtained by employing non-linear least squares methods, but that of Temkin and Dubinin–Radushkevich model are calculated by employing linear least squares approaches,[40] as summarized in Table 3.

Plots of q_e *versus* C_e for potassium adsorption are shown in Fig. S2(a) and (b).† It is obvious that the adsorption capacity increases with the initial concentration of the adsorbate and then reaches a platform after the adsorption sites are saturated. The adsorption capacities increase to some extent as the temperature drops. As shown in Table 3, the comparison between the coefficient values for various isotherm plots indicates that the Freundlich model with R^2 greater than 0.99 has the highest conformity. The value of n for potassium adsorption is 1.811 at 298 K, which is more than 1, indicating that it is favorable adsorption. The value of K_F increases with the decreasing temperature, indicating that low temperature is conducive to potassium adsorption. Moreover, the Langmuir model has the highest compliance with equilibrium data after the Freundlich model. When the initial concentration of potassium perrhenate was 2.00 g L^{-1}, the potassium concentration was 261.2 mg L^{-1}. According to eqn (S-2) in Text S1,† the dimensionless constant separation factor R_L value was calculated as 0.0028 at 298 K and was within the range of 0–1, indicating that the adsorption of potassium on the C160H resin was favorable. This result was consistent with that of the Freundlich model. The characteristic of the Freundlich model is its assumption that the active absorbent sites are heterogeneously distributed but they are homogenously distributed in the Langmuir model.[41,42] The Langmuir isotherm model also indicated the adsorption process develops as the monolayer coverage of the adsorbate, whereas the Freundlich isotherm model suggested the adsorption process was surface adsorption on the multilayer of the adsorbent.[43] Therefore, the adsorption of potassium by the C160H resin belongs to a multilayer and

RSC Advances
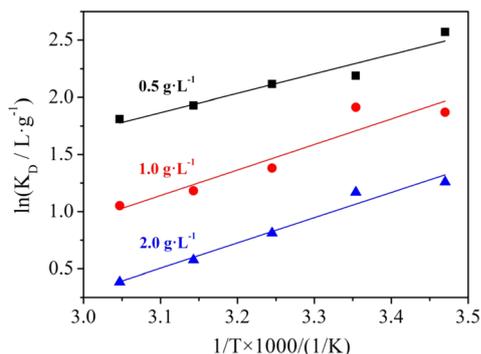
View Article Online

Paper

Fig. 5 Plot of ln K_D versus $1/T$ for the resin adsorbing potassium.

heterogeneous adsorption process. Besides, compared to the correlation coefficient R^2 in Table 3, the fitting sequence of the isotherm model was Freundlich > Langmuir > Dubinin–Radushkevich > Temkin.

3.3.2 Adsorption thermodynamics. The adsorption thermodynamics of the C160H resin toward K^+ were investigated by varying the ambient temperature and using 0.5 g L^{-1}, 1.0 g L^{-1} and 2.0 g L^{-1} of KReO$_4$ solution. As shown in Fig. 5, the value of ln K_D linearly increased with increasing $1/T$, indicating that low temperatures contributed to the adsorption reaction. It is consistent with the adsorption isotherm results above. The standard free energy change (ΔG^0), standard enthalpy change (ΔH^0) and standard entropy change (ΔS^0) of the resin were calculated using the following equations:[44]

$$K_D = \frac{q_e}{C_e} \tag{3}$$

$$\ln K_D = -\frac{\Delta H^0}{RT} + \frac{\Delta S^0}{R} \tag{4}$$

$$\Delta G^0 = \Delta H^0 - T\Delta S^0 \tag{5}$$

where K_D is adsorption equilibrium constant, L g^{-1}; T is the reaction temperature, K; R is the gas constant, 8.314 J mol^{-1} K^{-1}.

ΔH^0 and ΔS^0 can be calculated from the slope and intercept of ln K_D versus $1/T$ according to Fig. 5. The values of the thermodynamic parameters are summarized in Table 4. The adsorption process was spontaneous because of negative ΔG^0 at all temperatures. The ΔG^0 grew more negative with the decreased temperature, indicating that the low temperature is conducive to the adsorption reaction to proceed spontaneously.

The negative ΔH^0 value suggested that the adsorption activity of K^+ was exothermic. Generally, the reaction follows a dissociative mechanism for the ΔS^0 value greater than -10 J mol^{-1} K^{-1}, but an associative mechanism for a more negative value than -10 J mol^{-1} K^{-1}.[45] According to Table 4, the ΔS^0 values are less than -10 J mol^{-1} K^{-1}, indicating that the adsorption reaction follows an associative mechanism.

3.3.3 Adsorption kinetics. The adsorption kinetics was investigated by varying the contact time between the resin and 2.0 g L^{-1} of KReO$_4$ solution. To confirm the dominant adsorption mechanism, the Pseudo-first-order, Pseudo-second-order and Weber–Morris models were further used to fit the kinetic data. The fitting results are shown in Fig. 6(a)–(c). Fig. 6(a) showed that the C160H resin exhibited a fast adsorption speed toward K^+, reaching adsorption equilibrium within 60 min. Parizi et al.[17] verified the equilibrium time for potassium adsorption by the C100 resin as 120 min. Therefore, the C160H resin has faster potassium adsorption speed than the C100 resin, shortening the equilibrium time for potassium adsorption.

The kinetic parameters related to the Pseudo-first-order model are obtained by employing non-linear least squares methods, and that of Pseudo-second-order and Weber–Morris models are calculated by employing linear least squares methods.[44] The parameters obtained from the fitting plots are listed in Table 5, showing that the correlation coefficients of the Pseudo-second-order model reached 1 at 298 K, 308 K, 318 K and 328 K, and these values were better than those of the Pseudo-first-order and Weber–Morris models. Moreover, the calculated q_e from the Pseudo-second-order plot is close to the experimental data. These indicated that the adsorption process followed the Pseudo-second-order model and was dominated by chemical adsorption.[46,47] The obtained adsorption rate constant K_2 was further fitted using the Arrhenius equation, as shown in Fig. 6(d). The activation energy of the chemical potassium adsorption by the C160H resin was calculated as 31.178 kJ mol^{-1}.

Diffusion of K^+ ions from the bulk of KReO$_4$ solution into the C160H resin sites involves three stages: first, diffusion of the ions from the solution bulk to the layer surrounding the adsorbent; second, diffusion from this outer layer to the adsorbent surface; finally, diffusion from the surface to the internal sites.[41,48] The diffusion rate of the ions from the bulk solution to the adsorbent surrounding layer was fast by shaking (180 rpm), indicating that the main diffusion resistance of K^+ ions onto the C160 resin is probably the film and intra-particle diffusion. According to Fig. 6(c), the adsorption process is

Table 4 Thermodynamic parameters of potassium adsorption on the resins

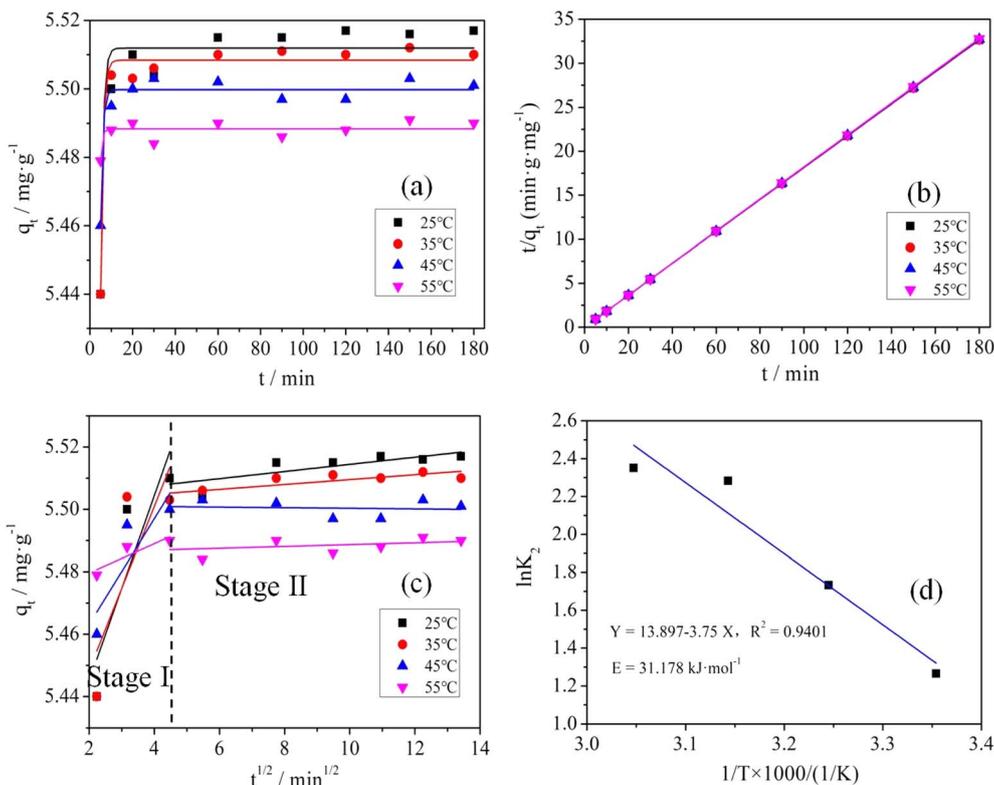| Concentration of KReO$_4$ solution/g L^{-1}	ΔH^0/kJ mol^{-1}	ΔS^0/J mol^{-1} K^{-1}	R^2	ΔG^0/kJ mol^{-1}				
				288 K	298 K	308 K	318 K	328 K
0.5	-14.078	-28.131	0.9436	-5.972	-5.691	-5.410	-5.128	-4.847
1	-18.601	-48.179	0.8997	-4.718	-4.236	-3.754	-3.272	-2.791
2	-18.365	-52.735	0.9726	-3.170	-2.642	-2.115	-1.588	-1.060

Fig. 6 Adsorption kinetics plots for K^+ adsorption on C160H resin. ((a) Pseudo-first-order; (b) Pseudo-second-order; (c) Weber–Morris; (d) plot of $\ln K_2$ versus $1/T$).

divided into two stages. It can be observed from Table 5 that the obtained intercept (C) is not zero, indicating that there is external film diffusion resistance at stage I.[46] Stage II corresponds to the intra-particle diffusion of K^+ ions in the C160 resin pores. Therefore, the fitting results of the Weber–Morris model indicate that the diffusion rate of potassium adsorption by the C160H resin is controlled by external film diffusion mixed with intra-particle diffusion.

3.4 Adsorption mechanism

FTIR spectra of the C160H resin before and after adsorption are shown in Fig. 7. The peaks at 3400 cm^{-1} and 2922 cm^{-1} are related to the vibrations of the hydroxyl group (–OH) and the antisymmetric stretching vibration of the –CH_2 group, respectively.[49,50] The peak at 1634 cm^{-1} refers to the C=C bond of the aromatic ring. The presence of the –SO_3H group in the C160H

resin can be identified by the characteristic peaks of this group at 1125 cm^{-1}, 1028 cm^{-1} and 670 cm^{-1}.[44] The peak at 1125 cm^{-1} occurs due to the asymmetric stretching vibration of the S=O bond, while the 1028 cm^{-1} peak refers to the symmetric stretching mode in the same bond.[51,52] The C–S bond between the polymeric carbon functional group of the resin and the –SO_3H group occurs at 670 cm^{-1}. The 830 cm^{-1} peak represents the attachment of the benzene ring of the divinylbenzene to sulfonic ion.[41] In addition, the peak at 548 cm^{-1} is related to the S–S bond.[53]

Fig. 7 shows that a specific absorption peak at 427 cm^{-1} corresponding to the O–K bond is detectable after adsorption in 1.0 g L^{-1} of $KReO_4$ solution, while this characteristic peak is absent in the C160H resin spectrum before adsorption. Moreover, the peak intensity of the O–K bond is increased after adsorption in 2.0 g L^{-1} of $KReO_4$ solution. According to the

Table 5 Kinetic parameters of K^+ adsorption by C160 resin from $KReO_4$ solution

|		Pseudo-first-order			Pseudo-second-order			Weber–Morris of stage I			Weber–Morris of stage II		
T/K	$q_{e,exp}$/mg g^{-1}	K_1/min^{-1}	q_e/mg g^{-1}	R^2	K_2/ g mg^{-1} min^{-1}	q_e/mg g^{-1}	R^2	$K_{p, I}$/ mg g^{-1} min$^{-0.5}$	C_I	R^2	$K_{p, II}$/ mg g^{-1} min$^{-0.5}$	C_{II}	R^2
298	5.406	0.867	5.512	0.9357	3.542	5.518	1	0.030	5.386	0.7786	0.001	5.503	0.6555
308	5.471	0.878	5.508	0.9797	5.655	5.512	1	0.026	5.396	0.6472	0.001	5.502	0.6913
318	5.765	0.985	5.500	0.9512	9.804	5.501	1	0.017	5.429	0.7639	0.000	5.501	0.0159
328	5.643	1.274	5.488	0.6139	10.498	5.490	1	0.005	5.470	0.8102	0.000	5.486	0.1439
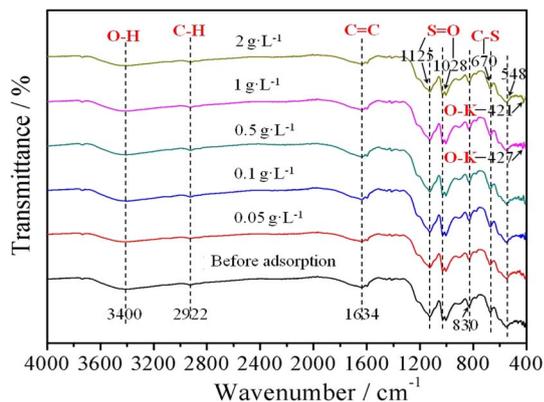
Fig. 7 FTIR spectrum of the C160H resin before and after adsorption at various concentrations of the KReO$_4$ solution.

Table 6 Mass percentage of each element in the C160H resin

	C%	H%	N%	S%	K%
Before adsorption	35.150	4.370	0	14.533	0.016
After adsorption	35.120	4.331	0	14.913	1.373

literature,[54,55] the characteristic peak of the O–K bond usually appears at 457 cm^{-1} or 520 cm^{-1}, and the neighboring atom of the O–K bond is the carbon atom. The peaks of the C–O and S–O stretching vibration are located at 1150 cm^{-1} and 1085 cm^{-1}, respectively.[56] However, the neighboring atom of the O–K bond is the sulphur atom in this work, and the peak of the O–K bond shifts to 427 cm^{-1} owing to the induced effect of the sulphur atom. Therefore, the potassium ion was successfully adsorbed on the C160H resin from the KReO$_4$ solution, and potassium was coordinated with the oxygen atom on the sulfonic acid group.

SEM-EDS were also used to examine the samples loaded with potassium, and the results are shown in Fig. S3.† Compared with the C160H samples before adsorption (Fig. S4†), the potassium spectral peak appeared at 3–4 keV, which indicated that K$^+$ ions were adsorbed successfully on the C160H resin. Moreover, elemental analysis was conducted to confirm the change in hydrogen content; the potassium content was quantitatively analyzed by ICP-AES, and the results are shown in Table 6. The mass percents of hydrogen and potassium were 4.370% and 0.016% before adsorption. However, after the adsorption of potassium, the mass percents of hydrogen and
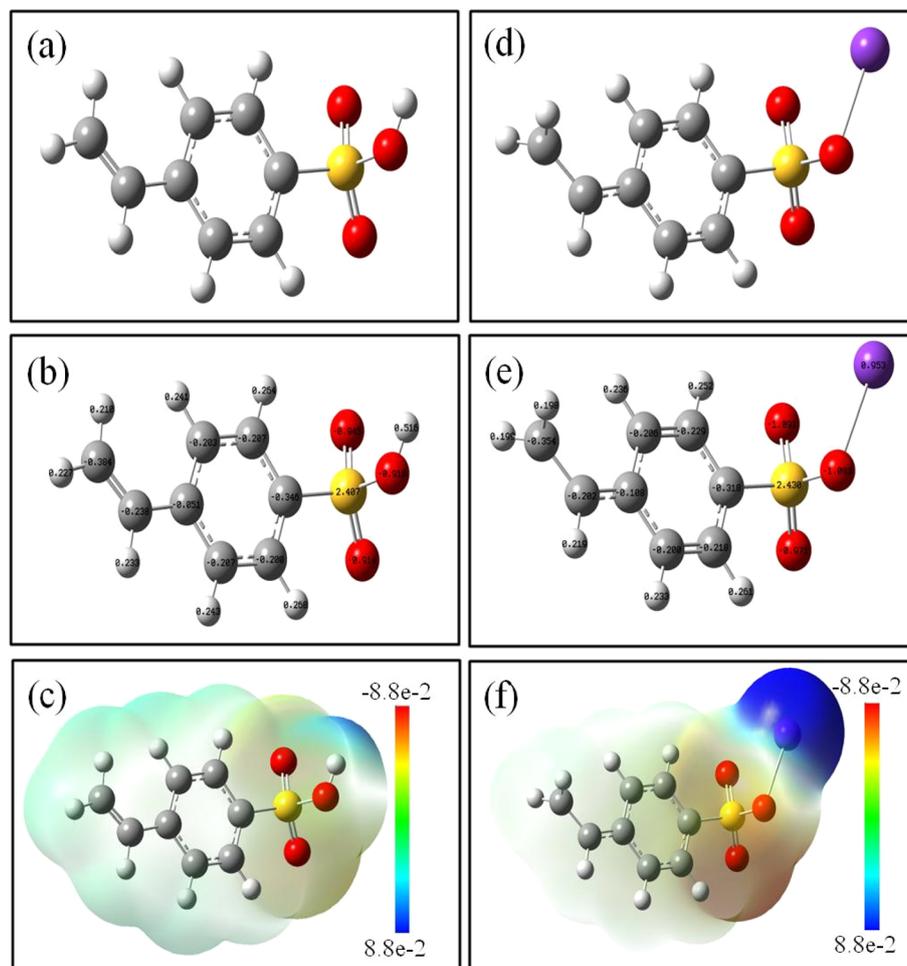

Fig. 8 Optimized structures, NBO charge distributions and molecular surface electrostatic potentials for 4-styrenesulfonic acid (a–c) and the complex binding with potassium (d–f). (O – red ball; S – yellow ball; C – grey ball; H – white ball; K – purple ball).
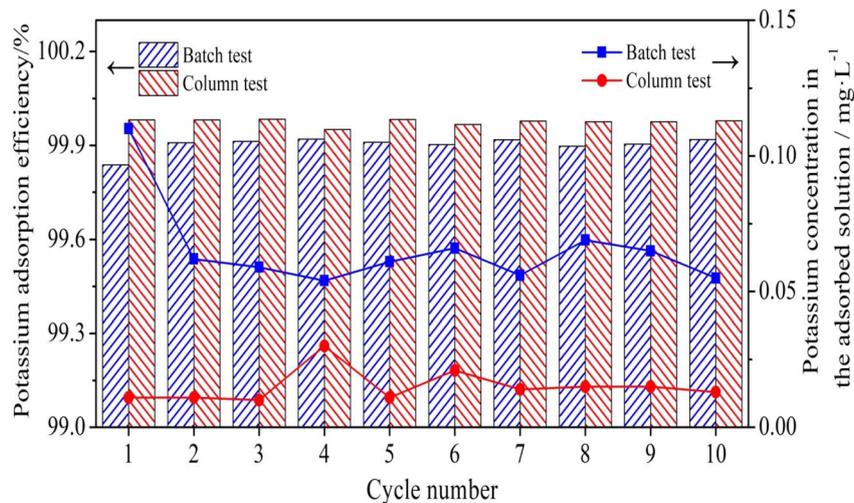
Fig. 9 Potassium adsorption efficiency on the C160H resin with the increasing cycle number (conditions for batch test: $KReO_4$ concentration = 0.5 g L^{-1}, initial pH = 7.0, temperature = 25 °C, rotating speed = 180 rpm, time = 6 h; conditions for column test: $KReO_4$ concentration = 0.5 g L^{-1}, initial pH = 7.0, temperature = 25 °C, flow speed = 20 mL h^{-1}).

potassium became 4.331% and 1.373%, respectively. The molar ratio of the decreased hydrogen amount to the increased potassium amount was calculated as $(4.370–4.331)/1 : (1.373–0.016)/39$, which was about 1 : 1, indicating that one H^+ ion was released for every K^+ ion adsorbed. Therefore, it is demonstrated that the adsorption mechanism of the C160H resin towards potassium is based on the cation exchange between H^+ and K^+.

To further investigate the interaction mechanism, DFT calculations were performed using the simplified structure, 4-styrenesulfonic acid, and the results are shown in Fig. 8. The results of structural optimization in Fig. 8(a) and (d) show that the adsorption of potassium by the C160H resin is accomplished by exchanging hydrogen on the sulfonic acid group with potassium, rather than with hydrogen in other locations. It is consistent with the FTIR spectrum analysis results.

As shown in Fig. 8(b) and (e), the negative charges were mainly shared by the oxygen atom of the sulfonic group, resulting in negative electrostatic potential around this region. This indicated that the oxygen atoms readily attracted positive cations and played important roles in the adsorption of K^+. Moreover, the positive charge of the potassium atom was 0.953, which was more positive than that of the hydrogen atom. Fig. 8(c) and (f) show that the electrostatic potential around the potassium atom was more positive than that of the hydrogen atom. These indicate that there is a stronger electrostatic interaction between K^+ and ligand than that between H^+ and ligand. Therefore, the adsorption activity was dominated by electrostatic interaction.

The calculation of binding energy (Fig. S5†) shows that the binding energy between H^+ and the ligand is 321.24 kcal mol^{-1} and that of K^+ with the ligand is 5.43 kcal mol^{-1}, further demonstrating that the coordination between K^+ and the ligand was much stronger than that between H^+ and the ligand. The theoretical calculation results are in agreement with the experimental results, demonstrating that the C160H resin has

a good absorption effect on potassium. Generally, the adsorption mechanism of potassium by the C160H resin can be illustrated by a simple chemical equation as follows:

$$[Matrix - SO_3^- \cdot H^+] + K^+ = [Matrix - SO_3^- \cdot K^+] + H^+ \quad (6)$$
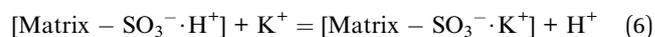
3.5 Regeneration performance

As shown in Fig. 9, the C160H resin has excellent regeneration performance during the batch test and column test. After ten adsorption–desorption cycles, the potassium adsorption efficiency still reaches 99.92% and 99.98% in the batch test and column test, respectively. The potassium concentration in the adsorbed solution decreased to less than 0.1 mg L^{-1}. Obviously, the regeneration performance of the C160H resin in the column test was better than that in the batch test. It is conducive to the subsequent industrial application of the C160H resin because the resin is loaded into the exchange column for adsorption and desorption in the actual industry.

4. Conclusions

In this work, the C160H resin was obtained and characterized after the commercial C160 resin was pretreated with 3 mol L^{-1} HNO_3 solution. The adsorption behavior and mechanism for potassium adsorption on the C160H resin from potassium perrhenate solution was demonstrated through adsorption isotherms, thermodynamics, kinetics modeling and DFT calculations.

The results showed that the mesoporous structure of the C160H resin was slightly improved, average pore size was 20.797 nm, specific surface area was 29.545 m^2 g^{-1}, but the PZC value was 1.63, which was lower than 6.19 of the C160 resin, resulting in the adsorption performance of the C160H resin towards potassium better than that of the C160 resin. At 25 °C,

the initial concentration of $KReO_4$ was 2.00 g L^{-1}, optimal pH of 7.0, solid-to-liquid ratio of 1:20 and time of 6 h, and the potassium adsorption efficiency of C160H was 99.28%. Moreover, the cation sequence affecting the potassium adsorption efficiency is $Na^+ < Ca^{2+} < Fe^{3+} < NH_4^+$.

The Freundlich model can fit the adsorption isotherm of potassium well, and the Freundlich constant of n is 1.811 at 298 K. The process is heterogeneous and favorable adsorption. The thermodynamic analysis suggests that the adsorption reaction is spontaneous and exothermic. The low temperature is conducive to the adsorption reaction. The potassium adsorption process follows an associative mechanism.

The adsorption process of potassium conforms to the pseudo-second-order kinetic model and is dominated by chemical adsorption, for which the activation energy is 31.178 kJ mol^{-1}. The diffusion rate of potassium adsorption by the C160H resin is controlled by external film diffusion mixed with intra-particle diffusion. The adsorption mechanism of the C160H resin towards potassium is based on the cation exchange between H^+ and K^+. During the potassium adsorption process, one H^+ ion is released for every K^+ ion adsorbed, and the electrostatic interaction is the dominant adsorption driving force. FTIR analysis verifies that the potassium atom is coordinated with the oxygen atom in the sulfonic acid group.

Compared with the C100 resin, the C160H resin exhibited a faster potassium adsorption speed, and the adsorption equilibrium time was shortened by 2 times, i.e., 60 min. Moreover, after ten adsorption–desorption cycles, the potassium adsorption efficiency still reached 99.92%, and the C160H resin has excellent regeneration performance. Although the maximum adsorption capacity of the C160H resin towards potassium is only 7.728 mg g^{-1} at 298 K in this work, according to the potassium adsorption mechanism, the capacity can be increased with the increased content of the sulfonic acid through sulfonation of the resin. On the whole, C160H resin is a promising choice for removing potassium from potassium perrhenate solution.

Data availability

The data supporting this article have been included as part of the ESI.†

Author contributions

Kunkun Chen: conceptualization, methodology, investigation, data curation, writing – original draft, funding acquisition. Linbo Li: conceptualization, writing – review & editing, resources, supervision. Kai Yang: methodology, writing – review & editing. Qigao Cao: writing – review & editing, supervision. Yunfei Chen: writing – review & editing, funding acquisition.

Conflicts of interest

The authors declare that they have no conflicts of interest.

Acknowledgements

References

1 U. Kesieme, A. Chrysanthou and M. Catulli, *Int. J. Refract. Met. Hard Mater.*, 2019, **82**, 150–158.

2 L. T. Shen, F. Tesfaye, X. B. Li, D. Lindberg and P. Taskinen, *Miner. Eng.*, 2021, **161**, 106719.

3 Y. Wang and C. Y. Wang, *Chin. Chem. Lett.*, 2018, **29**, 345–352.

4 R. P. Singh Gaur, T. A. Wolfe and S. A. Braymiller, *Int. J. Refract. Met. Hard Mater.*, 2015, **50**, 79–85.

5 X. Chen, Z. Tan, Y. F. Wu, Q. J. Zhang and D. A. Pan, *Therm. Sci. Eng. Prog.*, 2020, **19**, 100563.

6 A. M. Levin and O. M. Levchuk, *Russ. Metall.*, 2017, 47–53.

7 R. Lanam, A. Shchetkovskiy, A. Smirnov and E. Boland, *37th Joint Propulsion Conference and Exhibit*, Salt Lake City, 2001.

8 D. M. Rosenbaum, R. J. Runck and I. E. Campbell, *J. Electrochem. Soc.*, 1956, **103**, 518–521.

9 A. H. Zelikman, *Rare Metal Metallurgy*, ed. C. G. Song and Y. Z. Lu, Metallurgical Industry Press, Beijing, China, 1982.

10 K. Leszczyńska-Sejda, T. Majewski, G. Benke, J. Piętaszewski, K. Anyszkiewicz, J. Michałowski and A. Chmielarz, *J. Alloys Compd.*, 2012, **513**, 347–352.

11 A. N. Zagorodnyaya, Z. S. Abisheva, S. E. Sadykanova, A. S. Sharipova and A. Akcil, *Miner. Process. Extr. Metall. Rev.*, 2017, **38**, 284–291.

12 A. N. Zagorodnyaya, Z. S. Abisheva, L. Y. Agapova and A. S. Sharipova, *Theor. Found. Chem. Eng.*, 2019, **53**, 841–847.

13 A. N. Zagorodnyaya, A. S. Sharipova, K. A. Linnik and Z. S. Abisheva, *Theor. Found. Chem. Eng.*, 2018, **52**, 717–724.

14 A. A. Palant, V. A. Bryukvin, A. M. Levin and O. V. Reshetova, *Russ. Metall.*, 2011, 185–187.

15 L. Y. Agapova, E. I. Ponomareva and Z. S. Abisheva, *Hydrometallurgy*, 2001, **60**, 117–122.

16 K. Leszczyńska-Sejda, G. Benke, A. Chmielarz, S. Krompiec, S. Michalik and M. Krompiec, *Hydrometallurgy*, 2007, **89**, 289–296.

17 M. Torabi Parizi, A. Mostafavi and T. Shamspur, *J. Iran. Chem. Soc.*, 2023, **20**, 1469–1480.

18 R. Yagi and T. H. Okabe, *Int. Mater. Rev.*, 2024, **69**, 142–177.

19 M. B. Fathi, B. Rezai and E. K. Alamdari, *Int. J. Miner. Process.*, 2017, **169**, 1–6.

20 N. Nebeker and J. B. Hiskey, *Hydrometallurgy*, 2012, **125–126**, 64–68.

21 K. K. Chen, L. B. Li, Q. G. Cao and B. S. Zhang, *Rare Met. Mater. Eng.*, 2023, **52**, 345–350.

22 A. D. Lucas, P. CaÑIzares, J. F. Rodriguez and A. NuÑEz, *Solvent Extr. Ion Exch.*, 1996, **14**, 141–159.

23 P. J. Zhang, Z. G. Zhao, S. J. Yu, Y. G. Guan, D. Li and X. He, *Desalination*, 2012, **286**, 210–216.

24 A. Gołub and J. Piekutin, *Sci. Rep.*, 2020, **10**, 4624.

25 K. K. Chen, L. B. Li, Q. G. Cao and H. Q. Meng, *Rare Met. Mater. Eng.*, 2022, **51**, 3049–3056.

26 K. K. Chen, Q. G. Cao, H. Q. Meng, B. S. Zhang, P. C. Zhao and R. Dang, *Rare Met. Mater. Eng.*, 2021, **50**, 279–285.

27 E. Cristiano, Y.-J. Hu, M. Sigfried, D. Kaplan and H. Nitsche, *Clays Clay Miner.*, 2011, **59**, 107–115.

28 E. N. Bakatula, D. Richard, C. M. Neculita and G. J. Zagury, *Environ. Sci. Pollut. Res.*, 2018, **25**, 7823–7833.

29 L. Chen, J. Zhang, X. He, M. Liu, Q. Wei, X. Wang and Y. Wei, *Chem. Eng. J.*, 2020, **396**, 125300.

30 M. Branchi, M. Gigli, B. Mecheri, F. Zurlo, S. Licoccia and A. D'Epifanio, *J. Membr. Sci.*, 2018, **563**, 552–560.

31 G. Sposito, *Environ. Sci. Technol.*, 1998, **32**, 2815–2819.

32 C. M. Park, J. Han, K. H. Chu, Y. A. J. Al-Hamadani, N. Her, J. Heo and Y. Yoon, *J. Ind. Eng. Chem.*, 2017, **48**, 186–193.

33 S. V. Pochampally, E. Letourneau, I. Abdulraheem, J. Monk, D. Sims, S. E. Hunyadi Murph, E. J. Marti and J. Moon, *Chemosphere*, 2024, **367**, 143572.

34 M. Iqbal, A. Saeed and S. I. Zafar, *J. Hazard. Mater.*, 2009, **164**, 161–171.

35 D. Kołodyńska, J. Krukowska-Bąk, J. Kazmierczak-Razna and R. Pietrzak, *Microporous Mesoporous Mater.*, 2017, **244**, 127–136.

36 H. A. Alamudy and K. Cho, *Chem. Eng. J.*, 2018, **349**, 595–602.

37 E. R. Nightingale Jr, *J. Phys. Chem.*, 1959, **63**, 1381–1387.

38 R. J. Ma, *Ion Exchange Application in Hydrometallurgy,* Metallurgical Industry Press, Beijing, China, 1991.

39 S. Orda, M. Drzazga, K. Leszczyńska-Sejda, M. Ciszewski, A. Kocur, P. Branecka, K. Gall, M. Słaboń and M. Lemanowicz, *Materials*, 2023, **16**, 5481.

40 G. J. Millar, S. J. Couperthwaite and C. W. Leung, *Sep. Purif. Technol.*, 2015, **141**, 366–377.

41 H. Hajmohammadi, A. H. Jafari and M. Eskandari Nasab, *Iran. J. Chem. Chem. Eng.*, 2021, **40**, 1132–1147.

42 Y. P. Zhang, H. X. Zhu, X. Liu, T. Y. Fan, H. Liu, F. Wang and L. Deng, *Ion Exch. Adsorpt.*, 2020, **36**, 346–356.

43 S. V. Pochampally, J. G. Blanco, K. Ayalew, S. E. H. Murph and J. Moon, *Sep. Purif. Technol.*, 2024, **350**, 127793.

44 J. Tang, L. Liao, X. He, L. Lv, X. Yin, W. Li, Y. Wei, S. Ning and L. Chen, *Chem. Eng. J.*, 2024, **485**, 150022.

45 M. B. Fathi, B. Rezai, E. K. Alamdari and R. D. Alorro, *J. Min. Environ.*, 2018, **9**, 243–254.

46 Y. Sun, Y. Gu and J. Yang, *Chem. Eng. J.*, 2022, **428**, 131163.

47 S. Kang, B. Lee, K.-H. Ahn, S. Im, B. Kim, T.-H. Kim, Y. Hwang and S. Chae, *Chem. Eng. J.*, 2023, **457**, 141128.

48 F. Moghimi, A. H. Jafari, H. Yoozbashizadeh and M. Askari, *Trans. Nonferrous Met. Soc. China*, 2020, **30**, 236–248.

49 K. Wang, K. Chen, L. Xiang, M. Zeng, Y. Liu and Y. Liu, *Sep. Purif. Technol.*, 2022, **292**, 121044.

50 Y. Tian, X. Zhu, S. Zhou, W. Zhao, Q. Xu and X. Liu, *J. Bioresour. Bioprod.*, 2023, **8**, 198–213.

51 O. Ozer, A. Ince, B. Karagoz and N. Bicak, *Desalination*, 2013, **309**, 141–147.

52 J. H. Vinco, A. B. Botelho Junior, H. A. Duarte, D. C. R. Espinosa and J. A. S. TenÓRio, *Trans. Nonferrous Met. Soc. China*, 2022, **32**, 2438–2450.

53 S. Edebali and E. Pehlivan, *Powder Technol.*, 2016, **301**, 520–525.

54 C. Li, K. Wang, J. Li and Q. Zhang, *Nanoscale*, 2020, **12**, 7870–7874.

55 Q. Deng, Z. Luo, Y. Wang, H. Liu, Y. Zhou and R. Yang, *Mater. Lett.*, 2021, **301**, 130247.

56 C. Liu, X. Feng, Y. Zhao, H. Fan, R. Zheng, Z. Wang, H. Arandiyan, Y. Wang, S. K. Bhargava, Y. Liu, H. Sun and Z. Shao, *J. Colloid Interface Sci.*, 2023, **652**, 1325–1337.